Examination of Breast Phantom Layers Using UWB Antenna Sensing Technique

Original Scientific Paper

Sonal Patil*
Department of Electronics and Telecommunication Engineering
Ramrao Adik Institute of Technology, Nerul, Navi-Mumbai, India
sonalpatil606a@gmail.com

Khushboo Singh
Department of Computer Science and Design
New Horizon Institute of Technology, Thane, Mumbai, India
khushis7891@gmail.com

Ashwini Naik
Department of Electronics and Telecommunication Engineering
Ramrao Adik Institute of Technology, Nerul, Navi-Mumbai, India
ashwini.naik@rait.ac.in

*Corresponding author

Abstract *– Breast cancer is among the most prevalent cancers and is the second leading cause of cancer-related deaths in women globally. Early detection significantly improves treatment outcomes. Microwave sensing presents a non-invasive, cost-effective, and patient-friendly alternative, leveraging antenna sensors to detect variations in tissue dielectric properties. This work focuses on the design and development of a hexagonal ultra-wideband antenna and a breast phantom model to analyze different breast tissue types. The system comprising the antenna and phantom is modeled using the HFSS simulator and validated through experimental testing with a VNA. Variations in reflection characteristics are examined, as the microwave signals interact with breast tissues, revealing their lossy and dispersive nature through absorption, transmission, and reflection behavior. The antenna exhibited strong resonance across various phantom layers. System validation performed using the VNA indicates a simulated minimum return loss of –25.83 dB at 7.1 GHz and a measured value of –27.82 dB at 6.2 GHz. The presence of a tumor is identified through variations in reflection characteristics, and tissue properties such as the Specific Absorption Rate.*

Keywords*: MSA, HMSA, Breast phantom, Dielectric properties, UWB*

Received: June 26, 2025; Received in revised form: October 11, 2025; Accepted: October 13, 2025

1. INTRODUCTION

Breast cancer remains a leading cause of mortality among women worldwide, necessitating advanced diagnostic methods. Traditional imaging techniques often lack sensitivity in early-stage detection and may involve invasive or costly procedures. The disease typically results from genetic mutations and altered gene expression in breast tissue, accounting for approximately 10% of all newly diagnosed cancer cases worldwide each year. Early diagnosis is crucial for improving prognosis of the patient and treatment outcomes. Although widely used, standard tools like mammography and X-ray present limitations including high false-positive rates, reduced effectiveness in dense breast tissue, and exposure to ionizing radiation. MRI offers detailed imaging, particularly for patients with implants, but remains prohibitively expensive. Ultrasound aids in monitoring tumor progression and identifying various carcinoma types; however, its ability to detect small lesions is limited [1-4]. Microwave sensing provides a non-invasive and cost-effective approach to tumor detection, eliminating both ionizing radiation exposure and the need for breast compression. By assessing the electrical properties of biological tissues, it enhances detection accuracy, enables identification of small lesions, improves patient comfort, and reduces diagnostic errors. Microwave sensor arrays and biosensors play a vital role in breast imaging systems by improving cancer detection, enhancing image resolution, and enabling label-free diagnostics. These technologies offer distinct advantages over con-

ventional imaging methods [5, 6]. Conventional imaging modalities such as X-ray, MRI, and ultrasound have limitations in early breast cancer detection. An emerging solution is microwave sensing, which is valued for its safety, affordability, and patient comfort. Cancerous tissues exhibit higher permittivity, leading to increased microwave scattering, thereby making this method effective for detecting abnormalities. Antennas are key components in microwave sensing systems, with single-element sensors having omnidirectional radiation patterns that offer enhanced sensitivity, coverage in dense tissues, and simplified, cost-efficient system designs. Microwave sensing detects breast abnormalities by leveraging the contrast in dielectric properties between healthy and malignant tissues, as normal breast tissue is more transparent to microwaves, whereas tumors are more lossy due to higher fluid content. This study investigates the dielectric characteristics of various breast tissues by examining reflection responses using a microstrip antenna, extending the analysis of the antenna model presented in [7]. A hexagonal patch antenna and a heterogeneous breast phantom are proposed to evaluate the resonant behavior of breast layers across ultra-wideband frequencies. The structure of this work is as follows: Section 2 describes related work, Section 3 details antenna design and fabrication; Section 4 describes the breast phantom model and its construction; Section 5 presents experimental observations; and Section 6 concludes the study.

2. STUDY OVERVIEW

The tissue dielectric properties change after excitation due to temperature, dehydration, and ischemia, eventually stabilizing over time. In-vivo cancerous tissues exhibited higher dielectric values than ex-vivo samples, or Electrical Impedance Tomography measurements, although sample variability limits firm conclusions. Breast tumor detection depends on factors like tumor size and tissue permittivity, with interdependent effects— for example, return loss decreases with higher fibro permittivity but increases with greater skin and fat conductivity [8-10]. Ultra-wideband (UWB) and ultrasonic networks have the potential to transform in-body and near-body medical communications. Compared to traditional wireless systems, UWB provides higher data transfer speeds, lower power consumption, and enhanced security [11, 12]. Advanced UWB antennas—including open-mouth cut flower, bi-directional tapered slot, and inverted-F planar patch designs—have been developed. The incorporation of hard surface H-resonator arrays stabilizes radiation patterns, while combined single and circular complementary split ring resonators enable band rejection. Various human-body-compatible substrates were evaluated, however, the structures remain large and intricate [13, 14]. A multi-band antenna using FR-4 and RT-Duroid substrates with a defective ground structure demonstrated enhanced gain, bandwidth, and return loss; however, substrate thickness constrained its use in compact designs [16]. The planar octagonal UWB antenna, with circular slots in the radome and quarter-elliptical slots in the ground plane, achieves wide bandwidth while maintaining stable radiation characteristics [17]. Breast cancer detection was demonstrated using UWB antennas with patch configurations in dodecagon, square ring, circular, and hexagonal shapes; however, only simulated results were reported [18-24]. The Vivaldi antenna was used to classify breast tumors through microwave imaging. A 4×1 MIMO antenna array with elliptical patches was designed to operate across the ultra-wideband range and provide omnidirectional radiation. However, two of the reported antenna designs are found to be relatively large in size [25, 26]. Breast phantom design and fabrication are critical for system validation. Phantoms with fatty, skin, glandular, and tumorous layers are produced using common chemical mixtures. A technique integrating these tissues into a model accurately replicates physiological structure and dielectric properties. The materials exhibit durability and osmosis resistance, enabling fabrication of homogeneous and heterogeneous phantoms without compromising geometry or dielectric behavior. These phantoms are utilized for breast lesion detection and imaging in both narrowband and ultra-wideband frequencies [27, 28]. Hybrid machine learning and deep learning approaches have advanced breast cancer diagnosis. HH-AUSVM and feature selection achieved up to 97.97% accuracy, while the MI-CS-SBS/SFS-SVM model reached 99.5%. LSTM variants like HVSSFFLSTM showed strong performance, and FCM-based segmentation achieved high precision, with adaptability to other medical conditions. These complex models require GPU resources and involve high computational time, limiting their applicability for real-time use [29-32].

3. ANTENNA DESIGN

3.1. MICROSTRIP ANTENNA GEOMETRY

Microstrip patch antennas are highly attractive due to their compact size and lightweight design, making them well-suited for short-range applications. Conventional rectangular and circular patch antennas designed for the UWB spectrum typically resonate at a single frequency but offer limited bandwidth. These limitations render them inadequate for modern communication systems in their current form. To address these constraints, the antenna design is progressively modified into a hexagonal configuration. This design features a hexagonal patch on one side of the dielectric substrate and a ground plane on the opposite side. The simple structure of the microstrip antenna (MSA) makes it ideal for medical applications. Here, the design of a hexagonal microstrip antenna (HMSA) for UWB applications, as discussed in [7], is fabricated on a dielectric substrate made of double-sided copper flame-retardant epoxy glass composite. The HMSA structure is modeled and simulated using Ansys HFSS antenna

design software. The antenna is designed with a center frequency of 6.85 GHz, corresponding to a wavelength of 43.796 mm, enabling effective operation across the ultra-wideband spectrum from 3.1 GHz to 10.6 GHz.

The dielectric substrate of size 39.96 mm × 38.52 mm is made up of FR4 material with a thickness of 1.59 mm, a loss tangent of 0.02, and a relative permittivity (ε_r) of 4.4. Fig. 1 illustrates the antenna design, with detailed dimensions provided in Table 1.

The geometry of this compact design is straightforward and easy to fabricate. The HMSA is fabricated on an FR4 glass epoxy dielectric substrate measuring 40 mm × 40 mm. Printed technology is used to etch the metallic components, including the radiating patch, feed line, and ground plane. A 50 Ω coaxial probe feed supplies the structure, with an SMA connector used for connections. Fig. 2 shows the fabricated hexagonal microstrip patch antenna from both front and rear views.

Table 1. Design dimension details of HMSA

Parameter	SW	SL	h	GL	GW	PL	PW	FLL	FLW
Dimension (mm)	39.96	38.52	1.59	9	39.96	17.3	20	11.32	3

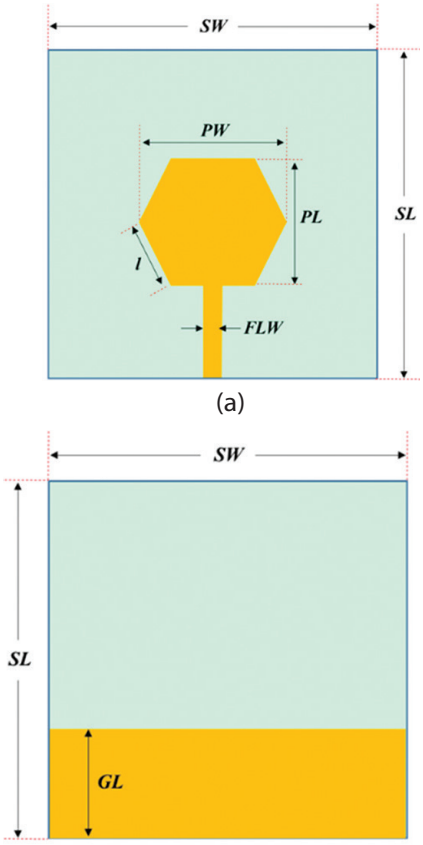

Fig. 1. Antenna Geometry of HMSA, (**a**) front perspective, (**b**) back perspective

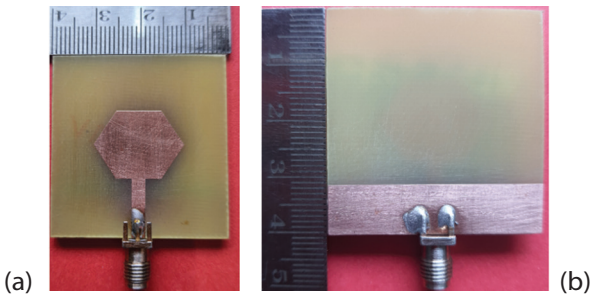

Fig. 2. Fabricated HMSA structure, (**a**) front perspective, (**b**) back perspective

The prototype was tested using a Vector Network Analyzer (model N9916A) to validate the results. The HMSA antenna exhibits a return loss below –10 dB, a VSWR below 2 across the frequency range of 3.1 GHz to 10.6 GHz, and a peak gain of 5.3 dB. Fig. 3 presents the reflection response of the HMSA based on both HFSS simulations and VNA measurements of the prototype. Fig. 4 presents gain variations of the antenna structure.

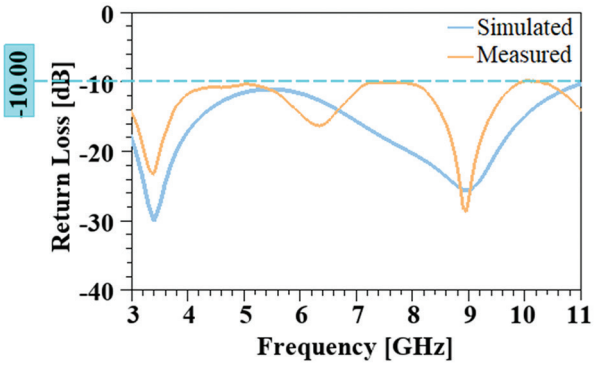

Fig. 3. Return Loss of Proposed Antenna

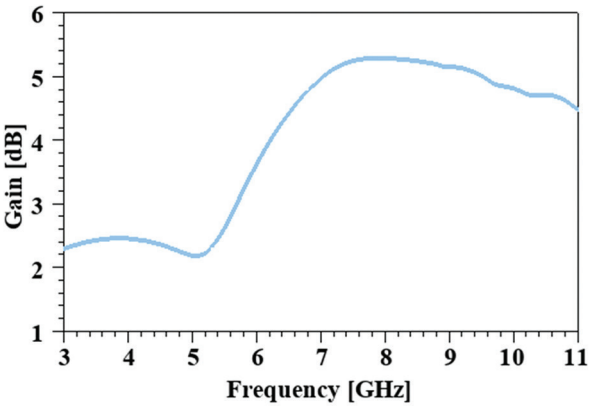

Fig. 4. Gain Variations of Proposed Antenna

4. BREAST PHANTOM

Phantoms are artificial replicas of body parts or organs designed to mimic the physical and structural characteristics of their biological counterparts. Breast phantoms

can be fabricated with varying tissue compositions to represent different tissue types. By accurately reproducing the three-dimensional distribution of adipose tissue layers, the breast model effectively simulates the properties of these tissues for microwave-based applications. The dielectric behavior of tissues is characterized by their permittivity and conductivity, with each breast layer exhibiting distinct lossy and dispersive properties. Layer 1 is the outermost skin layer. Layer 2 consists of fat or adipose tissue surrounding the glandular tissues. Layer 3 comprises glandular tissue, including milk ducts. Layer 4, shown in Fig. 5, represents tumor cells typically found in the lactiferous ducts and lobular membranes. Human breasts are classified as either homogeneous or heterogeneous based on tissue composition.

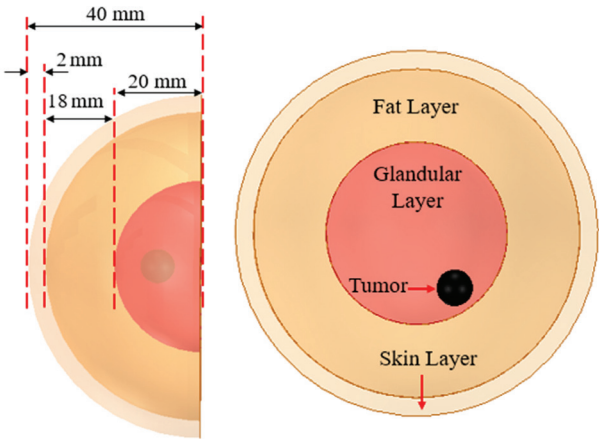

Fig. 5. Design Model of the Proposed Heterogeneous Breast Phantom (**a**) top perspective, (**b**) side perspective

4.1. MODEL DESIGN

The heterogeneous breast phantom consists of four distinct layers and is designed using Ansys HFSS software.

The design employs the single-pole Debye model to analyze tissue responses to frequency variations based on the dielectric properties of breast layers. The single pole Debye dispersion model is expressed as,

$$\varepsilon_r(\omega) = \varepsilon_\infty + \frac{\varepsilon_s - \varepsilon_\infty}{1+\omega^2\tau^2} \quad (1)$$

$$\sigma_r(\omega) = \frac{(\varepsilon_s - \varepsilon_\infty)\omega^2\tau\varepsilon_0}{1+\omega^2\tau^2} + \sigma_s \quad (2)$$

where,

ε_r - Complex permittivity,

ε_0 - Free space permittivity,

ε_s - Static dielectric constant,

ε_∞ - Dielectric constant at infinity,

σ_s - Static conductivity,

τ - Pole relaxation constant,

ω - Angular frequency

The breast model has a diameter of 40 mm, with a 2 mm thick skin layer, a 10 mm thick fatty layer, and a 28 mm thick glandular layer. The proposed antenna is used to evaluate the electrical characteristics across these breast tissue layers. Fig. 5 illustrates both the top and side views of the heterogeneous breast phantom design. The dielectric properties used for modeling each layer are based on frequency-dependent values, as summarized in Table 2. A 5 mm tumor is embedded in the glandular layer at a depth of 35 mm from the antenna center. The spacing between the antenna and the breast model is maintained at to 0.5 mm.

Table 2. Dielectric Properties of Breast Layers

Layer	ε_r	$\varepsilon\infty$	σ_s(S/m)	τ (ps)
Skin	4	37	1.10	7.37
Fat	6.57	16.29	0.262	7.00
Gland	47	76.31	0.46	7.00
Tumor	65	70	4	7.00

4.2. Phantom Materials

The heterogeneous breast phantom comprises four layers: skin, fat, glandular tissue, and an embedded tumor. Various materials cited in the literature are used to replicate breast tissue. For fabrication, the selected materials include safflower oil, distilled water, propylene glycol, agar-agar gelatin powder, formalin (37% formaldehyde solution), xanthan gum, and liquid detergent. Propylene glycol and safflower oil provide low conductivity, while distilled water increases permittivity. Xanthan gum acts as a thickener and, along with liquid detergent, serves as a surfactant. Formalin helps determine the melting point of agar-agar and stabilizes the phantom. Agar-agar gelatin mixtures offer dielectric properties similar to real breast tissue and are easy to fabricate with good mechanical strength. Despite varying chemical concentrations across layers, these materials simplify the phantom fabrication process. The specific compositions used are provided in Table 3, as referenced in [28].

Table 3. Material Composition for Heterogeneous Breast Phantom

Material	Quantity			
	Skin	Fat	Gland	Tumor
Distilled water (ml)	80	40	80	100
Safflower oil (ml)	14	39	21	7
Propylene glycol (ml)	7	2	7	7
Agar-agar gelatin (g)	7	8	6	12
Formalin (ml)	0.30	0.30	0.30	0.30
Xanthum gum (g)	2.5	2.5	2.5	2.5
Liquid detergent (ml)	0.30	0.30	0.30	0.30

4.3. FABRICATION STAGES

The phantom is constructed using identical base materials for all layers, with their specific concentrations detailed in Table 3. Fabrication begins by mixing distilled water and propylene glycol and, heating the solution in a double boiler at 90°C-100°C. Agar-agar gelatin powder

is then gradually added until fully dissolved. In a separate bowl, safflower oil is mixed with surfactants (xanthan gum and liquid detergent) and formalin (37% formaldehyde solution), then combined with the heated solution. Once the color changes, the mixture is removed from heat, stirred to avoid air bubbles, and cooled to 25°C before being poured into a mold and refrigerated overnight. To form the skin layer, a second bowl is placed 2 mm inside the first. After the mixture solidifies, the inner bowl is removed. The fatty layer is formed by placing a third bowl at a 20 mm radius from the outer bowl, resulting in an 18 mm thick layer. The glandular layer is then poured into the remaining space to form a 20 mm thick section, using the specified chemical composition. Two 5 mm diameter straws are inserted to simulate tumor regions. A pinch of different food color is added to the mixture to differentiate the layers visually. Fig. 6 illustrates the fabrication steps and the final heterogeneous breast phantom with an embedded tumor.

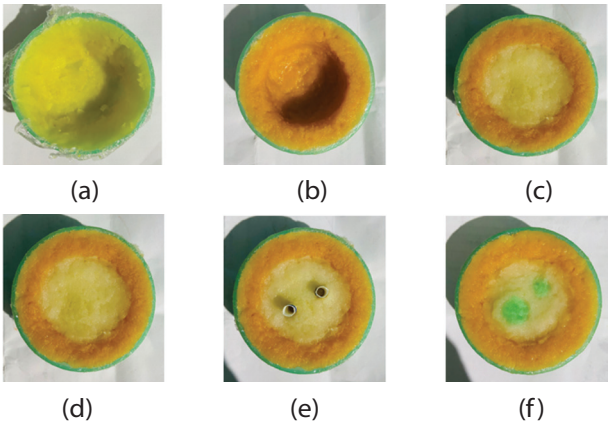

Fig. 6. Fabrication stream for Heterogeneous Breast Phantom, (**a**) Skin Layer, (**b**) Fatty Layer, (**c**) Gland Layer, (**d**) Breast Phantom without Tumor, (**e**) Provision to embed tumor, (**f**) Breast Phantom with Tumor

5. RESULT ANALYSIS

The principle of microwave sensing for breast lesion detection relies on the dielectric properties of tissues. Tumorous regions exhibit a significant dielectric contrast compared to normal breast layers. Radiation emitted from the antenna sensor propagates through the breast, interacting with each tissue layer.

To accurately represent the electrical behavior of breast tissues, their dispersive nature must be considered, as they act as lossy and dispersive media for microwave propagation. The interaction of microwaves with these biological tissues results in absorption, transmission, and reflection. The system model, comprising the antenna sensor and breast phantom, was validated using a Vector Network Analyzer (VNA), model N9916A. The reflection characteristics were recorded over three separate trials conducted within one week. The results from HFSS simulations were compared against the average values obtained from VNA measurements.

Figs. 7 to 10 show the reflection characteristics versus frequency for both the simulated and fabricated structures, focusing on the skin, fatty, and glandular layers of the breast model. The results indicate that tumorous tissues absorb more electromagnetic energy than normal tissues due to their lossy and dispersive dielectric properties. Consequently, the tumor layer exhibits the highest return loss, underscoring a significant difference in reflection behavior between healthy and cancerous breast tissues.

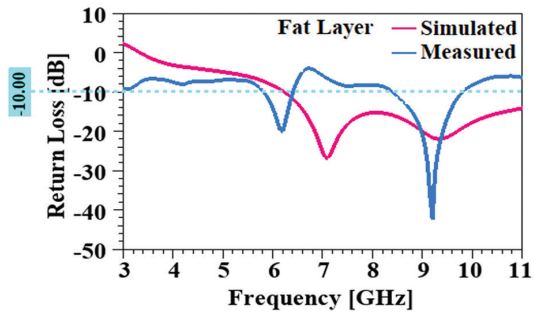

Fig. 7. Return Loss of Skin Layer

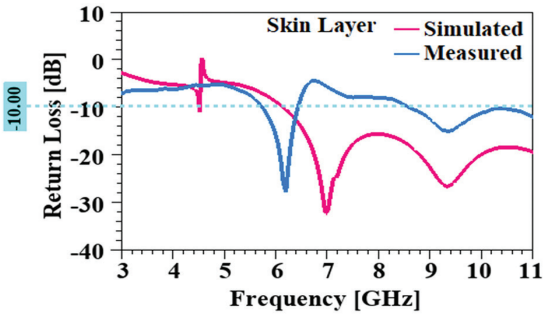

Fig. 8. Return Loss of Fatty Layer

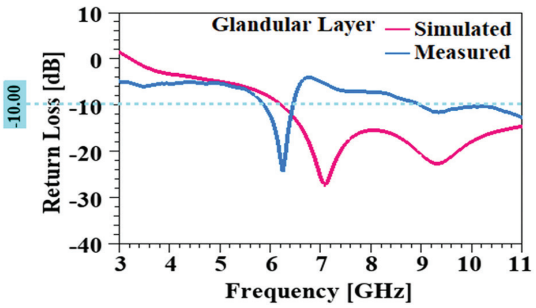

Fig. 9. Return Loss of Glandular Layer

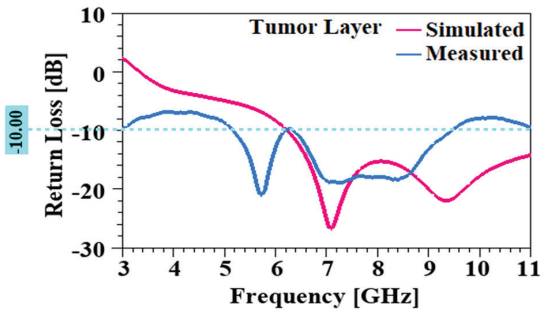

Fig. 10. Return Loss of Tumor Layer

Figs. 11 and 12 display the reflection characteristics of the system model, comprising the antenna and breast phantom, both with and without a tumor. A noticeable change in the reflection coefficient is observed, with the tumorous model showing higher return loss, allowing clear distinction from the healthy model. These breast phantoms provide a robust and adaptable platform for testing. The simulated structure exhibits a minimum S11 of –25.83 dB at 7.1 GHz, whereas the measured structure records –27.82 dB at 6.2 GHz. A performance comparison between the proposed phantom and similar models from the literature is provided in Table 4.

Table 4. Comparison with Existing Research

Ref. No.	Antenna Configuration	Antenna Size (mm2)	No. of Antenna Sensors	Gain (dB)	Bandwidth (GHz)	Reflection Coefficient S11 (dB)
[17]	Bi-Directional Tapered Slot Antenna for Imaging and UWB Applications	48 × 55	-	Not Reported	3.4 - 3.9 5 - 6	-28 (5.6 GHz)
[22]	Octagonal MSA with a Circular Slot, fed by a Tapered Strip Line, and an Elliptic Geometry Slot at Ground with reduced RCS for UWB Applications.	70 × 60	-	3.8	2.5 - 18	-41 (6.8 GHz)
[24]	Circular Patch Antenna for Breast Cancer Detection	48.46 × 42.46	1	2.453	2.5 - 3.4	-12.73 (2.876 GHz) -8.43 (2.36 GHz)
[26]	Hexagonal MSA for Breast Cancer Detection	25 × 20	1	Not Reported	3.1 - 10.6	-21.72 (5.6 GHz)
[27]	I-shaped Rectangular MSA with Two C-Slotted Parasitic Elements for Imaging Systems for Breast Cancer Detection.	40 × 30	1	2.45	4.9 - 7.89	-37 (8 GHz)
[28]	Rectangular MSA for Breast Tumor Detection using Microwave Radar-Based Imaging.	20.5 × 10.6	1	4.41	3 - 18	-19 (4.8 GHz)
[29]	Vivaldi Antenna with a Circular Holographic Structure for Microwave Imaging1	56 × 56	2	Not Reported	0.4 - 6.4	Not Reported
[30]	Four-Element, Elliptical-Shaped MIMO Antenna with Stubs on either side of the Ground for High Isolation in Breast Cancer Detection.	71.5 × 16	4 × 2	5.6	3.2 - 14	-22 (10.5 GHz)
Proposed Antenna	Simple Hexagonal MSA with Breast Phantom for Inspection of Breast Tissues.	39.96 × 38.52	1	5.3	3.1 - 10.6	-25.8343 (7.1 GHz) -27.8247 (6.2 GHz)

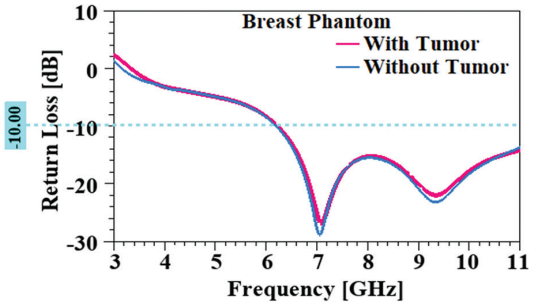

Fig. 11. Simulated S11 of Heterogeneous Breast

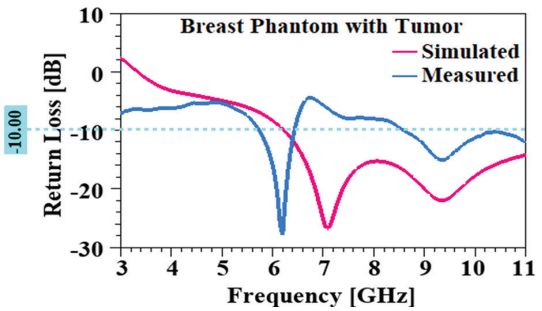

Fig. 12. Simulated Vs Measured of Heterogeneous Breast Phantom

The Specific Absorption Rate (SAR) is a metric that quantifies the rate at which electromagnetic energy emitted from a device is absorbed and converted into heat within a specific volume of human tissue.

Specific Absorption Rate is given by,

$$SAR = \frac{\sigma \, |E|^2}{\rho} \tag{3}$$

where, SAR - Specific Absorption Rate (W/kg),

σ - conductivity (S/m),

ρ - the mass density (kg/m3).

Tumorous tissues absorb more incident microwave energy than normal tissues. This absorption, measured as the SAR, serves as a useful indicator for detecting malignant tissues.

Fig. 13 illustrates the SAR distribution in the breast phantom for both healthy and tumorous tissues.

The SAR value is higher in tumorous regions due to greater absorption of electromagnetic energy.

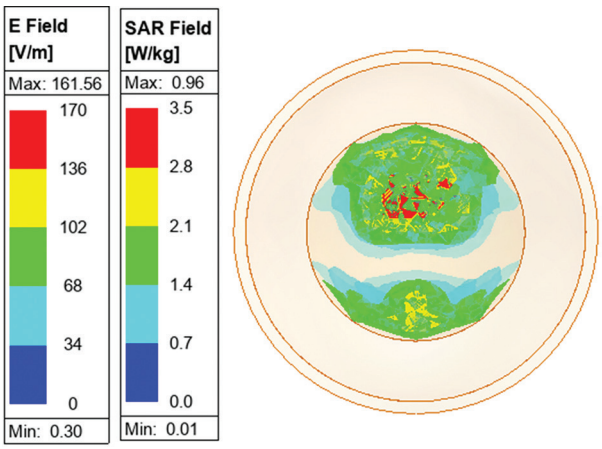

(a)

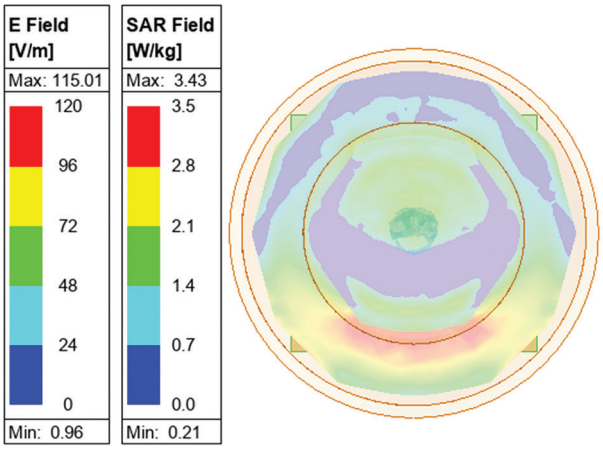

(b)

Fig. 13. SAR of Heterogeneous Breast Phantom (**a**) Healthy Breast, (**b**) Tumorous Breast

6. CONCLUSION

A hexagonal patch UWB antenna was fabricated on a double-sided copper FR4 epoxy glass substrate and tested using a Vector Network Analyzer (VNA) model N9916A. The HMSA antenna, designed in Ansys HFSS for a center frequency of 6.85 GHz ($\lambda = 43.796$ mm), was optimized for minimal return loss across the UWB spectrum, achieving a peak gain of 5.3 dB. It was employed to characterize the various tissue layers of a heterogeneous breast phantom, which comprised skin, fat, glandular, and tumor tissues. The phantom was modeled in HFSS and fabricated using a mixture of safflower oil, distilled water, propylene glycol, agar-agar gelatin, formalin, xanthan gum, and liquid detergent—selected for their ability to replicate realistic dielectric properties and maintain structural integrity. The antenna demonstrated strong resonance when interacting with different phantom layers. System testing with the VNA showed a simulated minimum return loss of –25.83 dB at 7.1 GHz and a measured value of –27.82 dB at 6.2 GHz. Tumor presence was identified through changes in reflection characteristics, and tissue properties such as the Specific Absorption Rate (SAR) were analyzed. Additionally, tumor localization was achieved by identifying regions of maximum power absorption. The integration of machine learning algorithms can further improve the accuracy of tumor detection.

REFERENCES

[1] R. L. Siegel, T. B. Kratzer, A. N. Giaquinto, H. Sung, A. Jemal, "Cancer Statistics", CA: A Cancer Journal for Clinicians, Vol. 67, No. 1, 2017, pp. 7-30.

[2] S. H Heywang Kobrunner, A. Hacker, S. Sedlacek, "Advantages and Disadvantages of Mammography Screening", Breast Care, Vol. 6, No. 3, 2011.

[3] E. C. Fear, P. M. Meaney, M. Stuchly, "Microwaves for Breast Cancer Detection", IEEE Potentials, Vol. 22, No. 1, 2003, pp. 12-18.

[4] S. G. Orel, M. D. Schnall, "MR Imaging of the Breast for the Detection, Diagnosis, & Staging of Breast Cancer", Radiology, Vol. 220, No. 1, 2001, pp. 13-30.

[5] L. Wang, "Microwave Sensors for Breast Cancer Detection", Sensors, Vol. 18, No. 2, 2018, p. 655.

[6] A. A. Maged, A. Khawla, S. A. Thamer, M. B. Saeed, A. Hussein, M. R. Omar, "Review of Microwaves Techniques for Breast Cancer Detection", Sensors, Vol. 20, No. 8, 2020.

[7] K. Singh, S. Patil, A. Naik, S. Kadam, "Hexagonal Microstrip Patch Antenna Design for UWB Application", Proceedings of the International Conference on Automation, Computing and Communication, ITM Web of Conferences, India, 2022, Vol. 44, p. 02004.

[8] E. Jones, M. O'Halloran, M. Glavin, "Anatomy and Dielectric Properties of Breast and Breast Cancer", Introduction To Microwave Imaging For Breast Cancer Detection, 2016, pp. 5-16.

[9] S. Kwon, S. Lee, "Corrigendum to Recent Advances in Microwave Imaging for Breast Cancer Detection", International Journal of Biomedical Imaging, Vol. 2, 2018, p. 1657073.

[10] N. Uncu, E. A. Aydin, "The Effects of Dielectric Values, Breast and Tumor Size on the Detection of Breast Tumor", Tehnički Glasnik, Vol. 13, No. 3, 2019, pp. 197-203.

[11] B. Sandipan, S. Mahasweta, N. Santosh, C. Suchismita, "A Survey on Ultra-Wideband and Ultrasonic Communication for Body Area Networks", Inter-

national Journal of Ultra Wideband Communications and Systems, Vol. 3, No. 3, 2016.

[12] X. Gao, L. Huai, "Modern Ultra-Wideband Communications: Recent Overview and Future Prospects", International Journal of Ultra Wideband Communications and Systems, Vol. 4, No. 2, 2020.

[13] A. H. Zaid, A. Adham, A. Mustafa, E. Taha, "A Modified Compact Bi-Directional UWB Taperd Slot Antenna with Double Band-Notch Characteristics", Advanced Electromagnetic, Vol. 8, 2019, pp. 74-79.

[14] T. A. Elwi, O. A. Tawfeeq, Y. Alnaiemy, H. S. Ahmed, N. Lajos, "A UWB Monopole Antenna Design based RF Energy Harvesting Technology", Proceedings of the Third Scientific Conference of Electrical Engineering, Baghdad, Iraq, 19-20 December 2018, pp. 111-115.

[15] S. Y. A. Fatah et al. "Design of Compact Flexible UWB Antenna Using Different Substrate Materials for WBAN Applications", Proceedings of the Photonics & Electromagnetics Research Symposium, Prague, Czech Republic, 3-6 July 2023. pp. 373-378.

[16] K. V. Prashanth, P. Hadalgi, P. Hunagund, "Comparative Investigation on Multi-Band Antenna using FR-4 and RT-Duroid", International Journal of Ultra Wideband Communications and Systems, Vol. 5, No. 1, 2022, p. 40.

[17] M. D. Cengizhan, C. Sibel, C. Gonca, "Planar Octagonal-Shaped UWB Antenna with Reduced Radar Cross Section", IEEE Transactions on Antennas & Propagation, Vol. 62, No. 6, 2014, pp. 2946-2953.

[18] M. Kahar, A. Ray, D. Sarkar, P. P. Sarkar, "An UWB Microstrip Monopole Antenna for Breast Tumor Detection", Microwave Optical Technology Letters, Vol. 57, No. 1, 2015, pp. 49-54.

[19] I. Amdaouch, O. Aghzout, A. Naghar, A. V. Alejos, F. Falcone, "Breast Tumor Detection System Based on a Compact UWB Antenna Design", Progress in Electromagnetics Research M, Vol. 64, 2018, pp. 123-133.

[20] A. Aziz et al. "On-Body Circular Patch Antenna for Breast Cancer Detection", Proceedings of the IEEE International Electromagnetics and Antenna Conference, Vancouver, BC, Canada, 17-19 October 2019, pp. 29-34.

[21] A. Kahwaji, H. Arshad, S. Sahran, A. G. Garba, R. I. Hussain, "Hexagonal Microstrip Antenna Simulation for Breast Cancer Detection", Proceedings of the IEEE International Conference on Industrial Informatics and Computer Systems, Sharjah, Dubai, United Arab Emirates, 13-15 March 2016, pp. 1-4.

[22] T. V. Padmavathy, P. Venkatesh, D. Bhargava, N. Sivakumar, "Design of I-shaped Dual C-slotted Rectangular Microstrip Patch Antenna (I-DCSRMPA) for Breast Cancer Tumor Detection", Cluster Computing, Vol. 22, 2018, pp. 13985-13993.

[23] E. A. Aydin, M. K. Keles, "UWB Rectangular Microstrip Patch Antenna Design in Matching Liquid and Evaluating the Classification Accuracy in Data Mining Using Random Forest Algorithm for Breast Cancer Detection with Microwave", Journal of Electrical Engineering & Technology, Vol. 14, 2019, pp. 2127-2136.

[24] G. S. Deepthy, M. Nesasudha, "Microstrip Antenna for Early-Stage Breast Cancer Detection - A Survey", Journal of Health and Technology, Springer, 2021, pp. 1191-1204.

[25] R. C. Conceicao, H. Medeiros, M. O'Halloran, D. Rodriguez-Herrera, D. Flores-Tapia, S. Pistorius, "Initial Classification of Breast Tumor Phantoms using a UWB Radar Prototype", Proceedings of the IEEE International Conference on Electromagnetics in Advanced Applications, Turin, Italy, 9-13 September 2013, pp. 720-723.

[26] P. K. Rao, R. Mishra, "Elliptical Shape Flexible MIMO Antenna with High Isolation for Breast Cancer Detection Application", IETE Journal of Research, Vol. 69, No. 1, 2023, pp. 325-333.

[27] E. Porter, J. Fakhoury, R. Oprisor, M. Coates, M. Popovic, "Improved Tissue Phantoms for Experimental Validation of Microwave Breast Cancer Detection", Proceedings of the Fourth European Conference on Antennas and Propagation, Barcelona, Spain, 12-16 April 2010, pp. 1-5.

[28] M. T. Islam, M. Samsuzzaman, S. Kibria, "Experimental Breast Phantoms for Estimation of Breast Tumor using Microwave Imaging Systems", IEEE Access, Vol. 6, 2018, pp. 78587-78597.

[29] V. Murugesan, P. Balamurugan, "Breast Cancer Classification by Gene Expression Analysis using Hybrid Feature Selection and Hyper-Heuristic Adaptive Universum Support Vector Machine", International Journal of Electrical and Computer Engineering Systems, Vol. 14, No. 3, 2023, pp. 241-249.

[30] E. J. Sweetlin, S. Saudia, "Performance Analysis of a new Filter and Wrapper Sequence for the Survivability Prediction of Breast Cancer Patients", International Journal of Electrical and Computer Engineering Systems, Vol. 14, No. 5, 2023, pp. 547-555.

[31] M. P. Behera, A. Sarangi, D. Mishra, "Enhancing Breast Cancer Diagnosis: A Hybrid Approach with Bidirectional LSTM and Variable Size Firefly Algorithm Optimization", International Journal of Electrical and Computer Engineering Systems, Vol. 15, No. 6, 2024, pp. 523-530.

[32] S. Shakir, Y. A. Hamad, R. Kareem, "Breast Pathology Changes Extraction and Measurement Based on Machine Learning and DWT", International Journal of Electrical and Computer Engineering Systems, Vol. 16, No. 2, 2025, pp. 153-161.